Basic Relationships in the Pre-Reforming of n-Hexane on Ni/MgO Catalyst

Francesco Arena
Dipartimento di Chimica Industriale e Ingegneria dei Materiali, Università degli Studi di Messina, Salita Sperone 31, I-98166 S. Agata (Messina), Italy

DOI 10.1002/aic.10888
Published online May 12, 2006 in Wiley InterScience (www.interscience.wiley.com).

*The activity-selectivity-stability pattern of a 19 wt% Ni/MgO catalyst in the pre-reforming of n-hexane (T, 450°C; P, 10-15 bar; S/C, 1.5-3.5), in the absence and the presence of H_2 (H_2/C, 1), is thoroughly addressed. C*oking *and, to a much lesser extent,* sintering *phenomena affect the catalyst stability with a* 1st-order *dependence of deactivation rate on activity. Regardless of reaction conditions, in the absence of hydrogen a general* selectivity-conversion *pattern signals that CO is a primary reaction product from the steam reforming reaction, whereas the prevalence of a hydrogenolysis path enhances reaction rate, methane selectivity, and catalyst stability in the presence of hydrogen, markedly hindering the coking process. Driven by different* ensembles *of active sites, steam reforming, CO methanation, water-gas-shift, hydrogenolysis, and coking functionalities control the behavior pattern of the Ni/MgO catalyst in the pre-reforming process.*
 AIChE J, 52: 2823–2831, 2006
Keywords: pre-reforming, Ni/MgO catalyst, coking, sintering, reaction mechanisms

Introduction

Hydrogen is nowadays a strategic chemical intermediate finding extensive use in numerous industrial processes from hydrocracking-hydrotreating in oil refining, to production of fine chemicals and synthesis of ammonia and methanol.[1-3] The actual hydrogen refinery balance, at present consistent with the needs of the chemical industry, is yet destined in the near future to inevitable deficits as there is an ever decreasing output from catalytic reforming, due to softening of the process severity for reduction of aromatics content in gasolines,[1,2] and rising demand of hydrogen/syngas for synthesizing more efficient and *cleaner* fuels (hydrogen, synthetic gasolines, dimethylether, and so on) from natural gas rather than oil.[4,5] Therefore, improving the economics of hydrogen/syngas production will be a pressing challenge for the chemical industry in the future.[1-3]

Exploitation of "combined" energy-effective reforming technologies[1-3,6] and continuous improvements of steam-reforming catalysts' performance and lifetime[6-10] are to date the main routes pursued. In this context, *adiabatic pre-reforming* is an established technology implying relevant economic and operational benefits on overall syngas production.[1,2,6,11] Put upstream of a tubular reformer, a *pre-reforming unit* enhances feedstock flexibility and production capacity, ensuring also superior energy efficiency.[1,2,6,11] Despite being increasingly relevant from the industrial point of view,[1,2,6,11] relatively little scientific concern has been focused on the steam reforming of higher hydrocarbons after the main findings of Rostrup-Nielsen and co-workers.[6,12,13] A renewed research interest in superior hydrocarbons steam reforming has been prompted in recent years by the need of improving catalytic performance under particularly demanding process conditions.[7-10,14-17] Then, basic investigations of the activity-stability pattern of representative Ni catalysts in the pre-reforming of LPG,[17] and liquid hydrocarbon(s),[14] addressed both thermodynamic and kinetic analyses of the reaction stream,[14] and carbon deposition,[17] to ascertain the dynamics of coking phenomena. A decrease in the activity coefficient of surface carbon species was evi-

Correspondence concerning this article should be addressed to F. Arena at Francesco.Arena@unime.it.

Table 1. Activity Data (t_0, 30 min) and Amount of Carbon Deposits on the "Spent" Catalysts (after 17.5 h) Under Different Reaction Conditions (T, 450°C)

Run	P_R (atm)	S/C	H_2/C	χ_{C6H14} (%)	Reaction Rate ($mol_{C6H14} \cdot s^{-1} \cdot g_{cat}^{-1}$)	S_{CH4} (%)	S_{CO2} (%)	S_{CO} (%)	S_{C2-C5} (%)	W_{Carbon} ($g \cdot g_{cat}^{-1}$)
a	10	1.5[a]	0.0	52.6	0.82E-3	54.9	42.6	2.5	—	1.32
b	10	2.8[a]	0.0	70.8	1.10E-3	55.4	43.1	1.5	—	0.96
c	10	3.5[a]	0.0	75.8	1.29E-3	56.2	42.5	1.3	—	0.89
d	10	2.8[b]	0.0	38.1	1.11E-3	38.6	59.3	2.1	—	1.23
e	10	2.8[b]	1.0	77.1	2.37E-3	97.8	1.1	0.2	0.9	0.03
f	15	2.8[a]	0.0	68.6	1.61E-3	59.7	39.2	1.1	—	0.75

[a]P_{C6H14}, 0.18 atm; GHSV, 679,000 h^{-1}.
[b]P_{C6H14}, 0.18 atm; GHSV, 1,358,000 h^{-1}.

denced,[14,17] and threshold values for H_2O/C and H_2/C ratios have been pointed out.[17] Furthermore, reforming catalysts with improved resistance against coking and/or poisoning phenomena under low steam-to-carbon (S/C) ratio or in the presence of S-compounds have been proposed.[7-10,15,16]

It is generally recognized that coking processes of Ni-based catalysts in steam reforming and methanation reactions proceed through common carbon intermediates leading to the formation of several types of deposits depending on operating conditions.[6,12-14,17-20] Despite the causes and origins of carbon deposition being known,[6,11,18-20] there is little work by way of modeling of catalytic deactivation by coking. Often undervalued, moreover, the effects of metal sintering on the active surface area of typical pre-reforming catalysts have been recently emphasized.[21]

Therefore, this work is aimed at disclosing basic relationships that could highlight both the effects of coking and sintering phenomena on the activity-selectivity-stability pattern of a typical Ni/MgO catalyst in the steam reforming of n-hexane at pre-reforming conditions.

Experimental Procedures

Magnesia-supported nickel catalyst (MPF, 19.1 wt% Ni) was prepared by incipient wetness impregnation of a "smoke" MgO powder (UBE Ltd., SA_{BET}, 30 $m^2 \cdot g^{-1}$) with an ethanolic solution of the $Ni(NO_3)_2$ salt. The catalyst was dried at 80°C and calcined at 400°C (16h) in order to prevent the formation of the $Ni_xMg_{(1-x)}O$ solid solution,[22] and further pre-reduced for 6h at 650°C under H_2 flow.[14]

Catalyst testing in the pre-reforming of n-hexane was performed at 450°C and a total pressure of 10-15 bar, using an *isothermal* "fixed bed" stainless steel microreactor (i.d., 6 mm), loaded with 25 mg catalyst sample, diluted with same-sized SiC in a 1/30 weight ratio.[14] Before reaction the catalyst had been heated at 450°C in an H_2 flow (100 *STP* $mL \cdot min^{-1}$; P, 1 bar) and further reduced *in situ* at such temperature for 1h. The reaction mixture, containing n-C_6H_{14} (1.8%), N_2 (8.0%), He (rest), and H_2O (16.2-37.8%), for a variation of the S/C ratio between 1.5 and 3.5, respectively, was fed at the rate of 283 (GHSV, 679,000 h^{-1}) or 566 (GHSV, 1,358,000 h^{-1}) *STP* $mL \cdot min^{-1}$. The effects of H_2 feeding (11.0%; H_2/C, 1.0) have been probed at the highest GHSV and an S/C ratio equal to 2.8. The reaction temperature was controlled by a thermocouple in contact with the catalytic bed, while the reactor stream was analyzed by a GC equipped with a three-columns analytical system connected to both TCD and FID detectors for permanent gases and hydrocarbons analyses, respectively.[14]

TEM analyses were performed using a *PHILIPS CM12 Transmission Electron Microscope* (point-to-point resolution, 0.3 nm) on "fresh" and "spent" catalyst samples, dispersed ultrasonically in ethanol and deposited over a thin carbon film supported on a standard copper grid. The Ni particle size distribution (PSD) was obtained from an average of 150-200 particles, and the average volume-area particle size calculated by the conventional statistical formula[21]:

$$\bar{d}_{AV} = \frac{\sum_i n_i d_i^3}{\sum_i n_i d_i^2} \tag{1}$$

Results and Discussion

Activity-selectivity-stability pattern

Activity data (t_0, 30 min) of the MPF catalyst in the pre-reforming of n-hexane at 450°C with varying GHSV, feed stream composition (P_{H2O} and P_{H2}), and total pressure are summarized in Table 1 in terms of hexane conversion (χ, %), reaction rate, product selectivity (S_X, %) and weight of carbon on "spent" (such as after 17.5 h of time-on-stream) catalyst samples (W_{Carbon}, $g \cdot g_{cat}^{-1}$).[14] In addition, all the relative activity ($\alpha = \chi/\chi_0$, the ratio between conversion at the time "t" and "t_0," respectively) with time-on-stream (A) and selectivity versus conversion (B) data are collected in Figure 1. Regardless of experimental conditions, a systematic catalyst deactivation, mostly in the absence of hydrogen, implies a regular decrease of conversion during t.o.s. according to an *exponential*–decay trend, the extent of which roughly parallels the amount of carbon on "spent" catalyst samples (Table 1). Moreover, driven by a multi-step reaction network involving steam reforming, water-gas-shift, hydrogenolysis, and methanation reactions,[6-18] the only C-containing products are CH_4, CO_2, and CO, their relative distribution depending both on feed stream composition and operating conditions (Table 1). Small amounts of C2-C5 hydrocarbons ($S_{C2-C5} < 1\%$) are detected only in the presence of hydrogen (Table 1).

Namely, in the absence of H_2 at a pressure of 10 atm and an S/C ratio of 2.8, the hexane conversion is equal to ca. 71%, corresponding to a reaction rate of 1.1 $mmol \cdot s^{-1} \cdot g_{cat}^{-1}$, while methane (54-56%) and carbon dioxide (42-44%) are the most abundant reaction products. Meanwhile, an easy attainment of equilibrium conditions of the water-gas-shift reaction ($CO + H_2O$

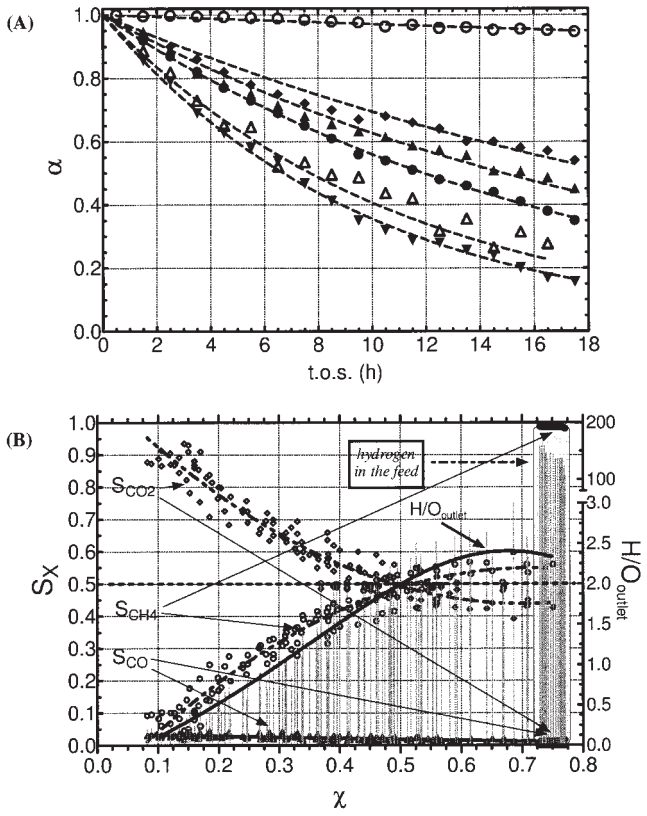

Figure 1. Pre-reforming of n-hexane (T, 450°C).

(a) Relative activity (α, χ/χ_0) with time-on-stream (t.o.s). Legend (see Tables 1 and 2): *run a* ▼; *run b* ●; *run c* ▲; *run d* △; *run e* ○; *run f* ◆. (b) Summary of product selectivity (S_X) and H/O_{outlet} ratio vs. hexane conversion data.

$\leftrightarrows CO_2 + H_2$) keeps CO at trace levels (0.2-2.5%).[7-10,14-17,23] Then, at a constant pressure of 10 atm, the most evident effects of a rise of the S/C ratio from 1.5 to 3.5 consist in a progressive improvement of hexane conversion (52.6 → 75.8%) and catalyst stability (Figure 1a), while a slight rise in S_{CH4} is offset by lower S_{CO2} (Table 1). A rise in total pressure from 10 to 15 atm (S/C, 2.8) implies a corresponding increase of reaction rate (1.61 $mmol_{C6H14} \cdot s^{-1} \cdot g_{cat}^{-1}$) and a further slight enhancement of S_{CH4} (59.7%) and catalyst stability (Figure 1a). Whereas a twofold increase of GHSV implies a proportional decrease of conversion and significant changes in the product distribution, evidenced by a decay in S_{CH4} from 55.4 to 38.6% (Table 1).

Irrespective of ongoing deactivation and experimental conditions, systematic changes in selectivity are in fact associated with the conversion level,[14,18-20,24-26] as documented by the general "selectivity-conversion" pattern depicted in Figure 1b. In particular, it shows that when the conversion of the substrate is low (ca. 10%), the main reaction products are CO and CO_2 ($S_{Cox} \approx 95\%$) in a molar ratio satisfying the thermodynamic equilibrium constraints of the WGS reaction,[11,14-18,23] while CH_4 is present in the outlet stream only at trace levels (≈5%). Thereafter, an increase of conversion up to 50% produces a corresponding rise in S_{CH4}, further leveling off smoothly to an asymptotic value of 55-60% in the conversion range 50-75% (Figure 1b). With an opposite specular trend, the S_{CO2} decreases from 90 to 45%, while the S_{CO} lowers, almost linearly, from ca. 2 to 0.5% in the whole conversion range (Figure 1b). These trends mirror marked changes in the ratio of hydrogen and oxygen atoms "contained" into reaction products, as the H/O_{outlet} increases from ca. zero until a steady value of 2.4 for conversion in excess of 50% (Figure 1b). Thus, the methanation functionality is enhanced at high conversion when almost all of the hydrogen from the splitting of water and cracking of hexane is converted to methane, resulting in a H/O_{outlet} ratio greater than two. In fact, the selectivity pattern shown in Figure 1b points to a reaction network involving the first occurrence of the hydrocarbon steam reforming with the primary formation of CO:

$$C_6H_{14} + 6H_2O \rightarrow 6CO + 13H_2 \qquad (a)$$

further transformed to CO_2 and CH_4, by parallel water-gas-shift (k_2) and methanation paths (k_4), respectively,[6-18,23,25,26]:

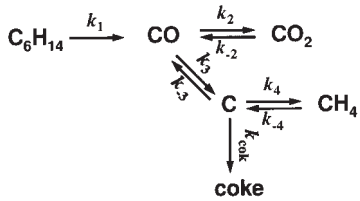

(I)

Adsorption and subsequent activation and decomposition of CO give rise to carbon species, the precursor of coke deposits build-up.[18,25,26] Definitively, the occurrence of a parallel or sequential hexane cracking step, leading to an intermediate formation of carbon species further undergoing gasification,[14,18,25,26]

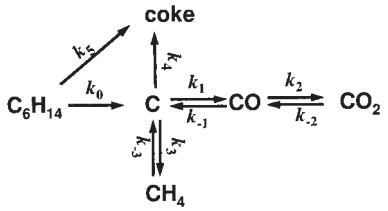

(II)

would not alter the fundamental essence of the reaction network. On this account, a rational explanation to the peculiar "conversion-selectivity" pattern in Figure 1b can be found in the potential of the gas-phase, since low CO and H_2 concentrations hinder the kinetics of CO methanation mostly at low conversion levels, while the WGS reaction always entails the prevailing formation of CO_2 in the presence of huge amounts of steam (Figure 1b). This becomes evident from the inspection of the "model" curves of the S_{CH4} and of the normalized H_2 yield ($[Y_{H2}]$, mol_{H2}/mol_C) versus conversion, shown in Figure 2. As the changes in the concentration of steam are virtually negligible at any conversion level (Figure 2), the analogous trends of S_{CH4} and $[Y_{H2}]^3$ curves matches with the consecutive methanation of CO

$$CO + 3H_2 \leftrightarrows CH_4 + H_2O \qquad (b)$$

that involves a direct 3rd-order relationship between methane and hydrogen concentration. Considering the minor variations

of the "{$(S_{CH4})/[Y_{H2}]^3$}" function in the whole conversion range (Figure 2), experimental findings confirm that the hydrogen pressure is the key-parameter accounting for the S_{CH4} trend with hexane conversion (Figure 1b). Moreover, since relevant amounts of carbonaceous deposits on "spent" catalysts (Table 1) parallel the rate of activity loss (Figure 1a), this being also inversely related to the initial conversion level (Table 1), it can be speculated that the methanation path acts as the main "competitor" of the coking process, enabling an effective gasification of the coke precursor species.[6,11,14,17-20,25,26] Then, in the absence of H_2, a same adsorbed "C" intermediate (such as $C\alpha$) coming from CO decomposition and/or steam reforming reactions,[18,25-29] could either undergo methanation or transformation into poorly reactive adsorbed species:

(a) amorphous carbon (C_β),
(b) vermicular carbon (C_V),
(c) bulk Ni carbide (C_γ), and
(d) crystalline, graphitic carbon (C_C),

precursors of carbonaceous deposits.[18,19,25,26]

Hydrogen in the feed stream in an H_2/C molar ratio of 1.0, indicated as the threshold value for avoiding carbon deposits build-up,[17,27] enables a 77% conversion at the highest GHSV (reaction rate, 2.45 $mmol_{C6H14} \cdot s^{-1} \cdot g_{cat}^{-1}$) along with an overwhelming selectivity to methane (S_{CH4}, 96-97%), resulting in a "selectivity-conversion" pattern evidently inconsistent with that in the absence of H_2 (Figure 1b). These evidences are diagnostic of an abrupt change in the main reaction pathway(s),[6,11,14,17,27] probed by the presence of C2-C5 hydrocarbons in the outlet stream and the marked enhancement of: (i) reaction rate (Table 1), (ii) H/O_{outlet} (Figure 1b), (iii) catalyst stability (Figure 1a), and (iv) resistance to coking (Table 1). Evidently, hydrogen in the feed inhibits the splitting of water driving mostly the hydrogenolysis of hexane while a competitive adsorption for the same metal sites adsorbing the carbon intermediates would prevent nucleation and growth of carbon deposits.[6,8,11-14,17,18,25-27]

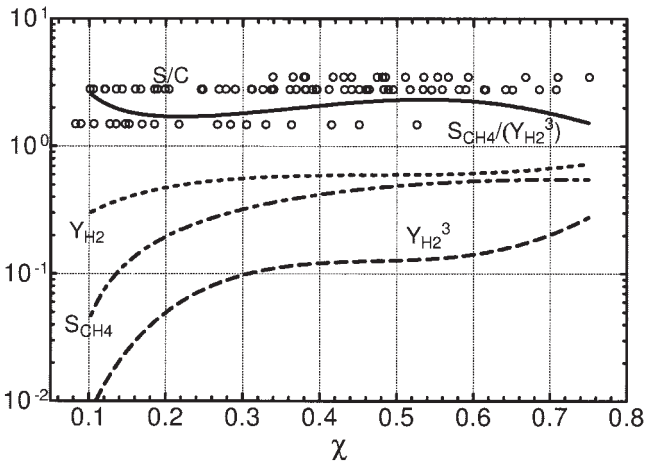

Figure 2. Pre-reforming of n-hexane (T, 450°C).

S/C (○) and S_{CH4}, Y_{H2}, and 237 $S_{CH4}/[Y_{H2}]^3$ 253 "model" function versus hexane conversion.

Modeling of coking, sintering, and deactivation phenomena

Several research articles recently addressed the effects of stream composition on coking[14,17,27] and sintering[21] processes of typical nickel catalysts at pre-reforming conditions. For instance, by adopting a thermodynamic approach, we shed light into the relative kinetics of forward and reverse equilibrium reactions involving carbon as reactant or product:

$$\text{GAS} \qquad C + H_2O \leftrightarrows CO + H_2 \tag{c}$$

$$\text{WGS} \qquad CO + H_2O \leftrightarrows CO_2 + H_2 \tag{d}$$

$$\text{MET} \qquad C + 2H_2 \leftrightarrows CH_4 \tag{e}$$

$$\text{DISP} \qquad 2CO \leftrightarrows C + CO_2 \tag{f}$$

In agreement with the fact that steam reforming/gasification and CO methanation proceed through a same C_α intermediate,[6,18,25,26] far away from equilibrium constraints,[14] the kinetics of forward gasification (GAS) and methanation (MET) lower during t.o.s. with a trend analogous to that of hexane conversion; whereas the kinetics of the Bouduard reaction ($2CO \leftrightarrows C + CO_2$), involving the carbon intermediate as a product, rises in a specular way.[14] Such data surmise a decrease of the carbon activity coefficient further to ageing, in agreement with the findings of Holmen and co-workers who developed kinetic equations of the steps involving the surface carbon intermediate to predict the dynamics of coking of a "model" Ni-aluminate catalyst in the pre-reforming of LPG.[17]

On the other hand, Datye et al. assessed the deactivation pattern by sintering of aluminate-supported Ni catalysts under pre-reforming conditions by evaluating the "long-term" kinetics of metal surface area decay at 500°C under an H_2O/H_2 stream.[21] From comparison of the PSD on "fresh" and "aged" catalysts, they argued the occurrence of the "*particle migration-coalescence*" sintering mechanism obeying to a 2nd-order kinetic relationship.[21]

Actually, comparative TEM views (Figure 3) of the "fresh" (a) and "used" (b and c) catalysts confirm the total absence of carbonaceous deposits on the spent catalyst in the presence of H_2 (Figure 3c), whereas catalyst particles in the absence of hydrogen are embedded into an intricate array of carbon fibers, 20-50 nm in diameter (Figure 3b).[6,11-17,25,29] A "smoothing" of the crystalline cubic habit of the magnesia carrier also reveals an incipient structure "restyling,"[11,21] coupled to a slight metal sintering probed by minor, though appreciable, changes in PSDs (Figure 3d). These signal a growth of the Ni particles diameter (d_{AV}) from 10.2 nm ("fresh" sample) to 10.9-11.2 nm on the "spent" catalysts, corresponding to a decrease in metal dispersion from ca. 10 to 9%, irrespective of H_2 feeding.

Such results entail that a reliable evaluation of the catalyst deactivation pattern must take into account both the effects of coking and sintering phenomena, though the effect of the latter is expected to be of much less importance.

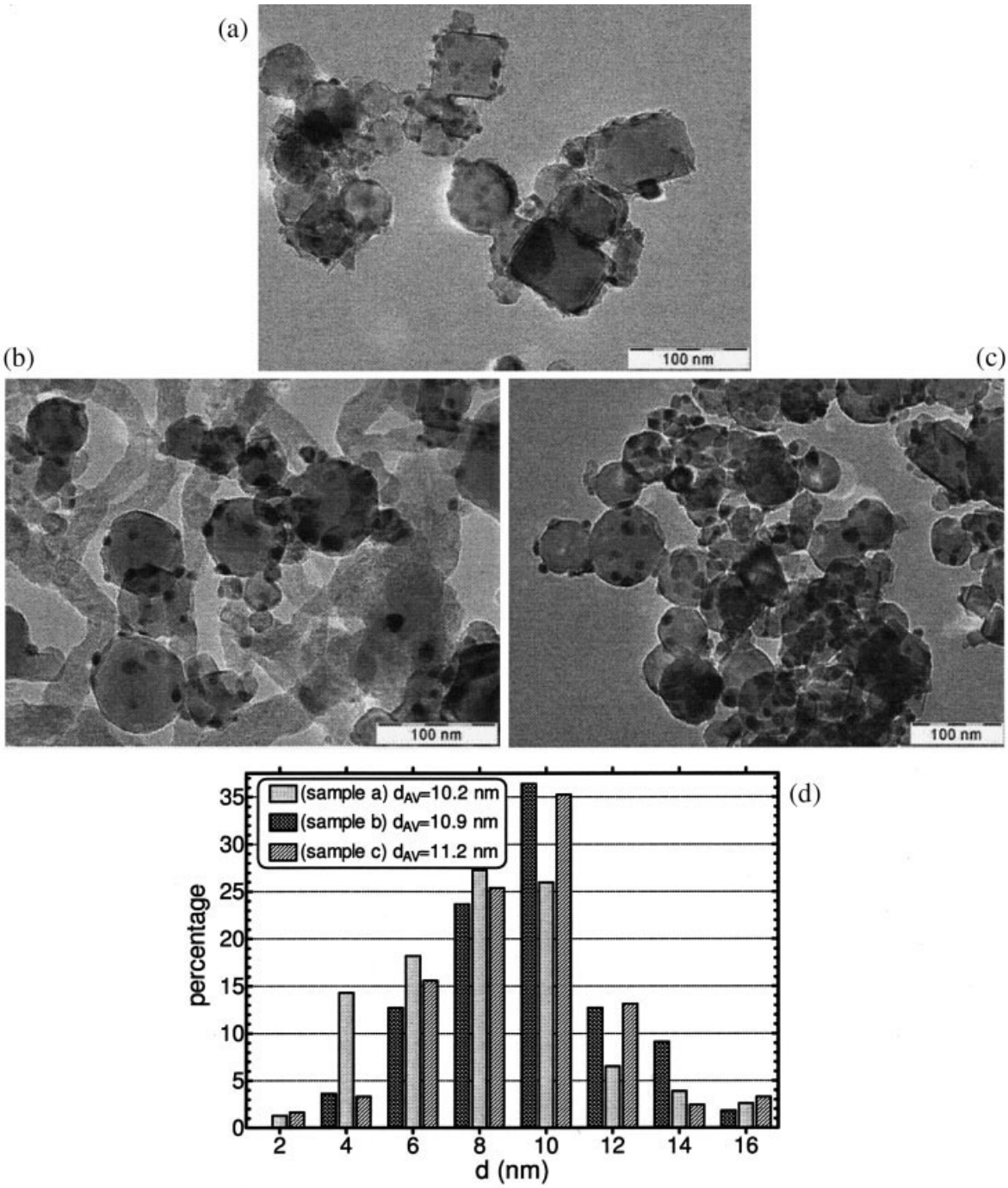

Figure 3. TEM micrographs (a-c) and PSD (d) of the "fresh" and "spent" catalysts.

Legend (see Tables 1 and 2): (a) "fresh" sample; (b) "spent" sample (run b); (c) "spent" sample (run e); (d) PSD of samples (a) through (c).

First, the exponential-decay fitting based on non-liner regression analysis of the relative activity data (Figure 1a)

$$\chi = \chi_0 \cdot e^{-k_{deact}t} \tag{2}$$

or

$$\alpha = e^{-k_{deac}t} \tag{3}$$

and already adopted for describing the activity decay by coking,[14] implies a 1st-order dependence of deactivation on activity

$$-\frac{d\chi}{dt} = k_{deact} \cdot \chi \tag{4}$$

finding a theoretic support in the extension of the "LHHW" kinetic approach to catalytic systems of changing activity.[20]

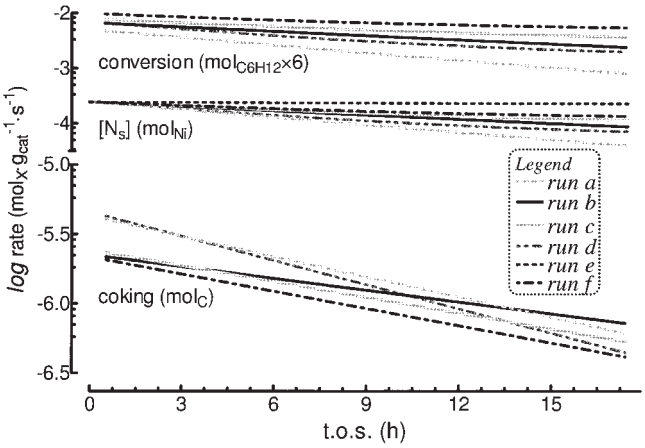

Figure 4. Pre-reforming of n-hexane (T, 450°C).

Hexane conversion, active sites disappearance, and coking rates versus t.o.s.

This can described on the basis of a simple reaction scheme including a surface intermediate (A^*) common to the formation of coke via a *parallel* path,[20]

$$A + * \underset{k_{-1}}{\overset{k_1}{\rightleftharpoons}} A^* \underset{k_{-2}}{\overset{k_2}{\rightleftharpoons}} B^* \underset{k_{-3}}{\overset{k_3}{\rightleftharpoons}} B + * \qquad \text{(III)}$$

$$k_{-4} \uparrow\downarrow k_4$$

$$\textit{coke}$$

and having the basic features of the above reaction networks (I)-(II). Then, the following assumptions must apply for predicting the effects of coking on active sites[20]:

(1) The surface reaction, $A^* \rightarrow B^*$, is the rate-determining-step ($k_{-1} < k_2 < k_1, k_{-2}, k_3, k_{-3}$), matching with the methanation step of the pre-reforming reaction network, as suggested both by the "selectivity-conversion" pattern and previous thermodynamic evaluations.[14]

(2) The rate of coking must be small in comparison to the reaction rate (that is, $k_4 < k_{-4} < k_2$). This requirement is also fulfilled according to Figure 4, showing in practice more than two orders of magnitude difference between reaction and coking rate at any condition and t.o.s.

(3) The rate of active site disappearance (deactivation) must be a linear function of the amount of coke (such as *unselective poisoning*).[19,20] The lack of intraparticle porosity,[22] avoiding major *pore-mouth plugging* phenomena,[18-20] allows the rate of active sites (such as $[N_s]$) disappearance of the studied catalyst to be in fact considered a linear function of the coking rate (Figure 4).

Therefore, a formal expression for the rate of active sites disappearance can be developed:

$$-\frac{dC_{site}}{dt} \propto \text{rate}_{cok} = \frac{k_4 K_A C_A C_{site}}{1 + K_A C_A + K_B C_B} \qquad (5)$$

This, upon integration at boundary conditions, becomes

$$C_{site} = C^0_{site} \cdot e^{\int k_4 K_A C_A/(1+K_A C_A + K_B C_B)dt} \qquad (6)$$

where $\mathbf{C_{site}}$ and $\mathbf{C^0_{site}}$ are the initial and final concentration of active sites. If the rate of coking does not depend on the concentration of the reacting species, the term under integer is constant and the rate expression becomes

$$\text{rate}_t = \text{rate}_0 \cdot e^{-k_{cok}t} \qquad (7)$$

with

$$k_{cok} = \frac{k_4 K_A C_A}{1 + K_A C_A + K_B C_B} \qquad (8)$$

Equations 2 and 3 satisfactorily accounted for the activity decay of the Ni/MgO catalyst in the pre-reforming of n-hexane,[14] since the effects of metal sintering were comparatively negligible. Indeed, as a representative case of deactivation by metal *sintering*, the slight activity loss in the presence of H_2 (≈7%) satisfactorily mirrors the metal surface area decrease (ca. 10%) evidenced by TEM analyses (Figure 3). This can be adequately described by an exponential-decay trend (Figure 1a), still pointing to a 1st-order dependence on activity or metal site concentration. Considering the strong interaction at the Ni-MgO interface,[22] which could effectively hinder the *migration-coalescence* sintering mechanism of Ni particles, this peculiar "low" kinetic dependence of the sintering rate on dispersion could be mostly the consequence of the ongoing reconstructuring of the MgO carrier (Figure 3) induced by the huge amount of steam in the feed stream (such as *steaming*).[11,19,21]

Then, in terms of conversion ($\chi \propto f(C_{site})$), the overall rate of the activity decay induced both by coking and sintering results:

$$-\frac{d\chi}{dt} = k_{cok} \cdot \chi + k_{sint} \cdot \chi \qquad (9)$$

Separating and integrating at boundary conditions, the obtained equation:

$$\alpha = \frac{\chi}{\chi_0} = e^{-(k_{cok} + k_{sint}) \cdot t} \qquad (10)$$

matches with the previous model equation,[14] provided that

$$k_{deact} = k_{cok} + k_{sint} \qquad (11)$$

If an asymptotic dispersion value is attained,[19,21] the integral equation rate becomes:

$$\alpha = \frac{\chi}{\chi_0} = \left(1 - \frac{k_{sint} \cdot \chi_\infty}{k_{deact}\chi_0}\right) \cdot e^{-k_{deact} \cdot t} + \frac{k_{sint} \cdot \chi_\infty}{k_{deact}\chi_0} \qquad (12)$$

Since $\boldsymbol{k_{sint} \ll k_{cok}}$ and $\chi_\infty \ll \chi_0$, the ratio

$$\frac{k_{sint} \cdot \chi_\infty}{k_{deact}\chi_0} \approx 0 \qquad (13)$$

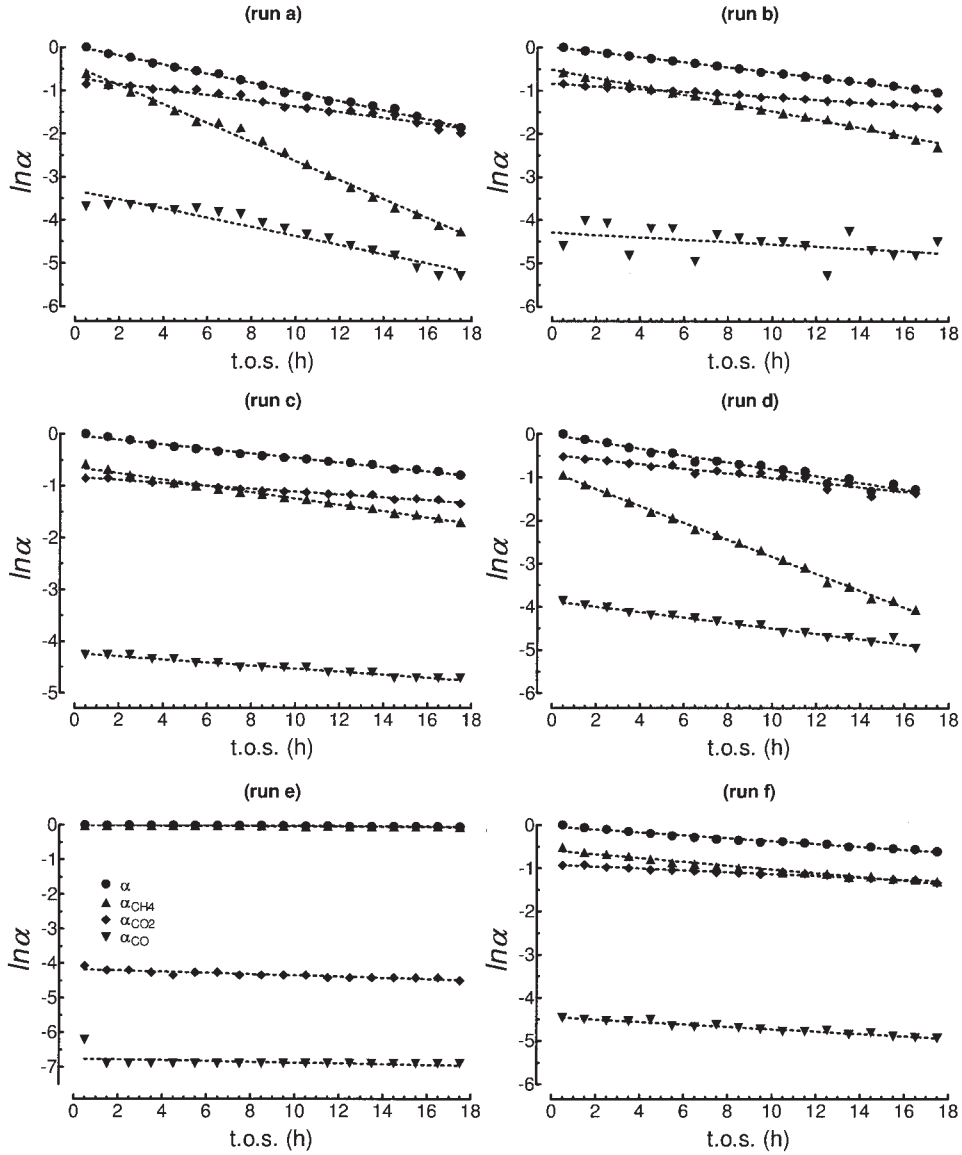

Figure 5. Pre-reforming of n-hexane (T, 450°C).

Relative rates of hexane conversion (α, ●), CH_4 (α_{CH4}, ▲), CO_2 (α_{CO2}, ♦), and CO (α_{CO}, ▼) formation vs. t.o.s. in the various runs (see Table 1).

Table 2. Deactivation Kinetic Constants of the Various Functionalities (*T*, 450°C): Hexane Conversion (k_{deact}), Methanation (k_{MET}), Gasification (k_{GAS}), Water-Gas-Shift (k_{WGS})

Run	k_{deact} (h^{-1})	k_{cok}[a] (h^{-1})	k_{MET} (h^{-1})	k_{GAS} (h^{-1})	k_{WGS} (h^{-1})
a	0.106	0.103	0.220	0.106	0.066
b	0.059	0.056	0.097	0.027	0.032
c	0.043	0.040	0.060	0.028	0.027
d	0.090	0.087	0.221	0.071	0.061
e	0.003	0.000	0.003	0.012	0.019
f	0.034	0.031	0.044	0.028	0.022

[a]$k_{cok} = k_{deact} - k_{sint}$ ($k_{sint} = k_{deact}$ in run e).

can be assumed negligible (see *infra*). Thus, the logarithmic form of integral Eqs. 10 and 12 results in any case in straight-line relationships (Figure 5), with the slope corresponding to the inverse value of k_{deact}. Likewise, the semi-log plot of the relative rates of product formation with t.o.s. results in all cases in fairly reliable linear trends (Figure 5). Then, the kinetic constant of the decay of the various functionalities in each run are summarized in Table 2. If the rate of sintering (run e) could be considered constant (for example, 0.003 h^{-1}) irrespective of the S/C ratio and total pressure, the effects of coking on activity are always prevalent, as indicated by k_{cok} values between 10 and 35 times greater than k_{sint} (Table 2). Accounting for coking and sintering processes, k_{deact} values yet match satisfactorily (±15%) with those quoted previously by non-linear regression of deactivation curves (Figure 1a), while the variations of the

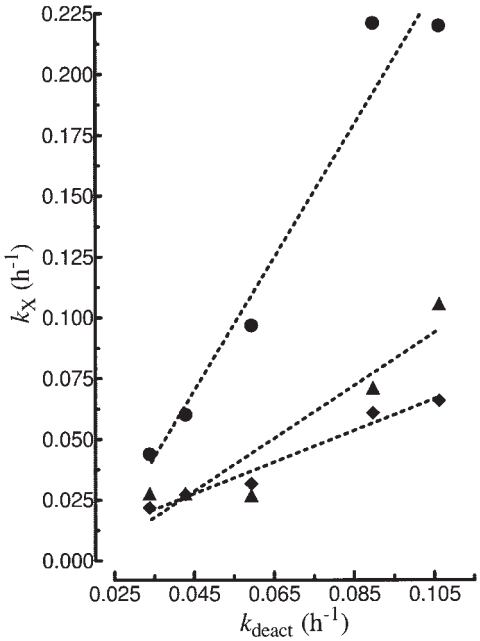

Figure 6. Pre-reforming of n-hexane (T, 450°C).

k_{MET} (●), k_{GAS} (▼), and k_{WGS} (◆) versus k_{deact} (see Table 2).

k_{cok} constant still entail an inverse dependence of the coking rate on the S/C ratio (that is, $k_{cok\infty}(P_{H2O})^{-1}$).[14]

Moreover, direct relationships between the kinetic constants of the various functionalities decay and that of activity loss result in straight-line correlations (Figure 6) with slope value equal to 2.7 (±0.3), 1.1 (±0.2), and 0.6 (±0.1) for methane, carbon monoxide, and carbon dioxide formation, respectively. Assuming that the relative activity is proportional at any time to the fraction of available sites (such as $\alpha = \chi/\chi_{0^\infty}C_{site}/C^0_{site}$), such figures would mirror the involvement of different *ensembles* of active sites by the various functionalities.[6,14,18-20,24-26] According to Froment et al. who adopted a stochastic approach to describe the deactivation functions with surface coverage by coking under different mechanisms,[24] MET (reaction e) is affected to the maximum extent by fouling of active sites owing to its highest *formal site molecularity* (*f.s.m.*),[28] in comparison to GAS (reaction c) and WGS (reaction d).[6,14,18,23] Anyway, the same slope value of the decay of hexane conversion and CO formation ($k_{GAS}/k_{deact} \approx 1$) supports the fact that the substrate likely undergoes a primary conversion to CO via the SR reaction.[6,11-14,17,18,25-28] The activity decay is then more enhanced at low conversion, mostly under the occurrence of SR-GAS and WGS reactions (Figure 1b), as the CO formation-decomposition is mainly responsible for carbon build-up via the adsorbed C_α intermediate[18,25]; whereas different reaction paths and deactivation mechanisms are probed by similar values of k_{deact} and k_{MET} (Table 2), and a much steeper decay of gasification ($k_{GAS}/k_{deact} \approx 3.5$) and WGS ($k_{WGS}/k_{deact} \approx 5$) functionalities in the presence of H_2.[6,14,18,27]

Conclusions

The activity-selectivity-stability pattern of the Ni/MgO catalyst in the pre-reforming of n-C_6H_{14} with steam, in the presence and absence of H_2, has been assessed.

A deactivation kinetic model based on a 1st-order kinetic dependence of concentration of active sites for both coking and sintering phenomena is outlined.

Basic relationships among activity, selectivity, and stability highlight a crucial role of the methanation path on the coking process and catalyst stability.

Coke formation in the absence of hydrogen occurs mostly via activation-decomposition of CO coming from the primary steam reforming reaction, while the hydrogenolysis path prevents build-up of carbonaceous deposits in the presence of H_2.

Literature Cited

1. Cromarty BJ, Hooper CW. Increasing the throughput of an existing hydrogen plant. *Int J Hydr En.* 1997;22:17-22.
2. Aitani AM. Processes to enhance refinery-hydrogen production. *Int J Hydr En.* 1996;21:267-271.
3. Fierro JLG, Peña MA, Gómez JP. New catalytic routes for syngas and hydrogen production. *Appl Catal A.* 1996;144:7-57.
4. Piel WJ. Transportation fuels of the future? *Fuel Process Tech.* 2001; 71:167-179.
5. Nagase S, Takami S, Hirayama A, Hirai Y. Development of a high efficiency substitute natural gas production process. *Catal Today.* 1998;45:393-397.
6. Rostrup-Nielsen JR, Alstrup I. Innovation and science in the process industry: steam reforming and hydrogenolysis. *Catal Today.* 1999;53: 311-316.
7. Suzuki T, Iwanami H, Yoshinari T. Steam reforming of kerosene on Ru/Al_2O_3 catalyst to yield hydrogen. *Int J Hydr En.* 2000;25:119-126.
8. Ming Q, Healey T, Allen L, Irving P. Steam reforming of hydrocarbon fuels. *Catal Today.* 2002;77:51-64.
9. Wang X, Gorte RJ. A study of steam reforming of hydrocarbon fuels on Pd/ceria. *Appl Catal A.* 2002;224:209-218.
10. Ayabe A, Omoto H, Utaka T, Kikuchi R, Sasaki K, Teraoke Y, Educhi K. Catalytic autothermal reforming of methane and propane over supported metal catalysts. *Appl Catal A.* 2003;241:261-269.
11. Christensen TS. Adiabatic prereforming of hydrocarbons—an important step in syngas production. *Appl Catal A.* 1996;138:285-309.
12. Rostrup-Nielsen JR. Activity of nickel catalysts for steam reforming of hydrocarbons. *J Catal.* 1973;31:173-179.
13. Rostrup-Nielsen JR. *Catalysis, Science and Technology*. Berlin: Springer-Verlag; 1983:5.
14. Arena F, Trunfio G, Alongi E, Branca D, Parmaliana A. Modelling the activity-stability pattern of Ni/MgO catalysts in the pre-reforming of n-hexane. *Appl Catal A.* 2004;266:155-162.
15. Suzuki T, Iwanami H, Iwamoto O, Kitahara T. Pre-reforming of liquefied petroleum gas on supported ruthenium catalyst. *Int J Hydr En.* 2001;26:935-940.
16. Chen F, Zha S, Dg J, Liu M. Pre-reforming of propane for low-temperature SOFCs. *Solid State Ionics.* 2004;166:269-273.
17. Sperle T, Chen D, Lødeng R, Holmen A. Pre-reforming of natural gas on a Ni catalyst. Criteria for carbon free operation. *Appl Catal A.* 2005;282:195-204.
18. Bartholomew CH. Carbon deposition in methanation and steam reforming. *Catal Rev-Sci Eng.* 1982;24:67-112.
19. Butt JB, Petersen EE. *Activation, Deactivation and Poisoning of Catalysts*. San Diego, CA: Academic Press, Inc.; 1998:1.
20. Forzatti P, Lietti L. Catalyst deactivation. *Catal Today.* 1999;52:165-181.
21. Sehested J, Carlsson A, Janssens TVW, Hansen PL, Datye AK. Sintering of nickel steam-reforming catalysts on $MgAl_2O_4$ spinel supports. *J Catal.* 2001;197:200-209.
22. Arena F, Horrell BA, Cocke DL, Parmaliana A, Giordano N. Magnesia-supported nickel catalysts. I: Structure and morphological properties. *J Catal.* 1991;132:58-67 and references therein.

23. Spencer MS. On the activation energies of the forward and reverse water-gas shift reaction. *Catal Lett.* 1995;32:9-13.
24. Beeckman JW, Nam I-S, Froment GF. Stochastic modelling of catalyst deactivation by site coverage. *Stud Surf Sci Catal.* 1987;34:365-379.
25. Jackson SD, Thomson SJ, Webb G. Carbonaceous deposition associated with the catalytic steam-reforming of hydrocarbons over nickel alumina catalysts. *J Catal.* 1981;70:249-263.
26. Snoeck J-W, Froment GF, Fowles MJ. Filamentous carbon formation and gasification: thermodynamics, driving force, nucleation, and steady-state growth. *J Catal.* 1997;169:240-249.
27. Sidjabat O, Trimm DL. Nickel-magnesia catalysts for the steam reforming of light hydrocarbons. *Top Catal.* 2000;11/12:279-282.
28. Fujita S, Terenuma H, Nakamura M, Takezawa N. Mechanisms of methanation of CO and CO_2 over Ni. *Ind Eng Chem Res.* 1991;30:1146-1151.
29. Tracz E, Scholz R, Borowiecki T. High-resolution electron microscopy study of the carbon deposit morphology on nickel catalysts. *Appl Catal.* 1990;66:133-148.

Manuscript received Oct. 12, 2005, and revision received Mar. 30, 2006.